THESIS FOR THE DEGREE OF LICENTIATE OF ENGINEERING

Chemical Doping of Conjugated Polymers for Thermoelectric Applications

Mariavittoria Craighero

CHALMERS

Department of Chemistry and Chemical Engineering

Division of Applied Chemistry

CHALMERS UNIVERSITY OF TECHNOLOGY

Göteborg, Sweden, 2023

Chemical Doping of Conjugated Polymers for Thermoelectric Applications

Mariavittoria Craighero

Thesis for the degree of Licentiate of Engineering

Nr. 2023:12

Department of Chemistry and Chemical Engineering

Division of Applied Chemistry

Chalmers University of Technology

SE-41296 Göteborg

Phone: +46 (0)31 772 1000

Cover: Schematic of a thermoelectric generator in the center surrounded by the chemical stuctures of conjugated polymers and dopants used in this thesis and by a schematic of the investigated properties.

Chalmers Reproservice

Göteborg, Sweden 2023

This project has received funding from the European Union's Horizon 2020 resear ch and innovation programme under the Marie Skłodowska-Curie grant agreement No 955837.

Chemical Doping of Conjugated Polymers for Thermoelectric Applications

ABSTRACT

The ongoing development of interconnected and wearable small devices, which together make up the so-called Internet of Things, is driving a rising need for autonomous and on-site energy supplies. Heat, an abundant and often wasted energy source, can be harnessed through thermoelectric generators that can directly convert heat into electricity. Small devices, such as health-monitoring sensors, may be powered by the heat dissipated from the human body using flexible thermoelectric generators made of organic semiconductors, like conjugated polymers.

This thesis discusses polythiophenes with oligoether side chains, which are a promising class of conjugated polymers for the design of flexible, easily processable and light-weight thermoelectric generators.

At first, this thesis investigates the solid-state order of these polymers and how is affected by varying the length of the oligoether side chains and by chemical doping with an oxidizing agent, F_4TCNQ, and an acid, H-TFSI. It is showed that inducing order, either by shortening the side-chain length or by doping, enhances the transport properties of the materials, and so their thermoelectric performance.

Secondly, this thesis studies the relationship between the solid-state order of these polymers and their mechanical properties. It is found that electrical and mechanical properties are usually correlated. The induced solid-state order not only improves the electrical conductivity but also enhances the stiffness of the materials. Partial decoupling of the electrical and mechanical properties is found to be possible if a suitable dopant is selected.

Keywords: *organic thermoelectrics, conjugated polymers, chemical doping, solid-state order, mechanical properties*

NOMENCLATURE

AcN	acetonitrile
$CHCl_3$	chloroform
DMA	dynamic mechanical analyzer
DSC	differential scanning calorimetry
EA	electron affinity
E_g	bandgap
EBSA	2-ethylbenzenesulfonic acid
F_2TCNQ	2,5-difluoro-7,7,8,8-tetracyanoquinodimethane
F_4TCNQ	2,3,5,6-tetrafluoro-7,7,8,8-tetracyanoquinodimethane
$FeCl_3$	iron(III) chloride
GIWAXS	Grazing Incidence Wide-Angle X-ray Scattering
HOMO	highest occupied molecular orbital
H-TFSI	bistriflimidic acid
I_2	iodine
IE	ionization energy
IoT	internet of things
LUMO	lowest unoccupied molecular orbital
$Mo(tfd\text{-}COCF_3)_3$	molybdenum tris[1-(trifluoroacetyl)-2-trifluoromethyl)ethane 1,2 dithiolene]
P3AT	poly(3-alkylthiophene)
P3BT	poly(3-butylthiophene)
P3DDT	poly(3-dodecylthiophene-2,5-diyl)
P3HT	poly(3-hexylthiophene)
P3OT	poly(3-octylthiophene-2,5-diyl)
PA	polyacetylene
PDMPV	poly(2,5-dimethoxy-p-phenylenevinylene)
PEDOT	poly(3,4-ethylenedioxythiophene)
PET	polyethylene terephthalate
TEG	thermoelectric generator
UV-vis-NIR	ultraviolet-visible-near infrared
ZT	figure of merit

PUBLICATIONS

This thesis consists of an extended summary of the following appended papers:

Paper I **Impact of oxidation-induced ordering on the electrical and mechanical properties of a polythiophene co-processed with bistriflimidic acid**

Sandra Hultmark, Mariavittoria Craighero, Sepideh Zokaei, Donghyun Kim, Emmy Järsvall, Furqan Farooqi, Sara Marina, Renee Kroon, Jaime Martin, Igor Zozoulenko and Christian Müller

Journal of Materials Chemistry C, **2023**, 11, 8091-8099

https://pubs.rsc.org/en/content/articlelanding/2023/TC/D2TC03927C

Paper II **Impact of oligoether side-chain length on the thermoelectric properties of a polar polythiophene**

Mariavittoria Craighero, Jiali Guo, Sepideh Zokaei, Sophie Griggs, Junfu Tian, Jesika Asatryan, Joost Kimpel, Renee Kroon, Kai Xu, Juan Sebastian Reparaz, Jaime Martín, Iain McCulloch, Mariano Campoy-Quiles, and Christian Müller

ACS Applied Electronic Materials, **2023**

https://pubs.acs.org/doi/10.1021/acsaelm.3c00936

The author has published the following papers which are not included in the thesis:

Paper III **Electrically conducting elastomeric fibers with high stretchability and stability**

Sepideh Zokaei, Mariavittoria Craighero, Claudia Cea, Lucas M. Kneissl, Renee Kroon, Dion Khodagholy, Anja Lund, Christian Müller

Small, **2022**, 02102813

Paper IV **Mechanically adaptive mixed ionic-electronic conductors based on a polar polythiophene reinforced with cellulose nanofibrils**

Mariza Mone, Youngseok Kim, Sozan Darabi, Sepideh Zokaei, Lovisa Karlsson, Mariavittoria Craighero, Simone Fabiano, Renee Kroon, and Christian Müller

ACS Applied Materials & Interfaces, **2023**, 15, 28300-28309

CONTRIBUTION REPORT

Paper I	Co-author. Preparation of samples for mechanical properties measurements. Contributed to data analysis and wrote part of the paper.
Paper II	Main author. Experimental design, solution processing and preparation of all samples. Optical spectroscopy, electrical and thermoelectrical measurements, thermal conductivity measurements and mechanical properties measurements. Data analysis, fitting optical spectra and calculations of doping efficiency, fitting thermal conductivity data. Wrote most of the paper.

TABLE OF CONTENT

Chapter 1

INTRODUCTION

1.1 Thermoelectric generators

As the global demand for energy production and management continues to increase, there is a growing interest in finding more effective and sustainable ways to generate power. Improvements to the existing energy supply must come from a variety of renewable sources including solar, wind, biomass, and others. Another potential source of energy is waste heat, which can be exploited using thermoelectric generators (TEGs).

These devices can harvest waste heat from various processes, such as industrial and automotive combustion, geothermal processes, or biological ones in the body, and convert it directly into electrical energy.[1-3] For instance, the electrical energy produced by TEGs can find application for powering sensors to monitor volcanic activity[4] or supporting the extensive network of distributed and interconnected microelectronics that make up the Internet of Things (IoT).[5] Therefore, thermoelectric technologies may contribute to increase the energy efficiency of many processes and to reduce waste by providing an autonomous and continuous source of energy.

TEGs are able to generate electrical power because they are constructed with thermoelectric materials that have the intrinsic capability of generating an electrical potential difference when exposed to a difference in temperature via the so-called Seebeck effect.

1.2 Organic thermoelectric generators

Thermoelectric generators rely on active materials that are primarily semiconductors, which can be either inorganic (such as bismuth telluride or lead telluride) or organic (such as conjugated polymers or small molecule organic compounds).

Inorganic thermoelectric materials find application as TEGs in sectors where a high thermal stability and durability are requested, for example in automotive industries. Instead, organic

thermoelectric generators can step in when flexibility and low-power requirements are demanded, e.g. for IoT devices or wearable technologies.

The distinct advantages of organic thermoelectric semiconductors lie in their ease of processability, largely through solution- and melt-based processing methods enabling their shaping in thin and bulk structures, and in their mechanical flexibility, which allows them to be integrated into wearable TEGs and curved surfaces (see Table 1.1). Additionally, their properties can be tailored through a modification of the chemical structure of the material. Conversely, inorganic semiconductors require complex and precise manufacturing processes, making their fabrication more challenging, and typically they are rigid and lack flexibility, which can limit their use in thermoelectric applications requiring conformability.

TEGs made of organic thermoelectric materials are characterized by lightweight, low cost and generally not-toxicity. Organic semiconductors for TEGs can unlock the potential to harness low-grade heat gradients, such as the temperature difference between the human body and its surroundings, generating electrical energy for power health-monitoring sensors.[6]

Table 1.1. Properties of organic and inorganic thermoelectric generators.

Property	Organic TEGs	Inorganic TEGs
Raw materials	based on carbon, hydrogen, and other elements like nitrogen, oxygen, and sulfur (abundant elements)	natural non-renewable sources (minerals and rare earth elements)
Processability of raw materials	cost-effective solution- and melt-based methods	advanced and precise fabrication processes
Mechanical properties of raw materials	flexibility	rigidity
Scalability	high	medium
Performance	low/medium	high
Thermal stability	low	high
Weight	low	medium/high
Toxicity	generally non-toxic	may contain toxic elements
Cost	low	high

1.3 Aim and scope

This thesis aims to establish relevant structure-property relationships with regard to the thermoelectric and mechanical properties of p-doped polythiophenes.

The work focuses on the impact of chemical doping and side-chain length on the nanostructure of thin films and how these affect the final electrical conductivity and thermoelectric performance of the material. Two different p-doping methods, (1) acid doping with bistriflimic acid (H-TFSI) (**paper I**) and (2) redox doping using the common oxidizing agent 2,3,5,6-tetrafluoro-7,7,8,8-tetracyanoquinodimethane (F_4TCNQ) (**paper II**) are investigated, the later for a series of three polymers with different side-chain lengths.

Besides this, the mechanical robustness and flexibility of free-standing films of the p-doped polythiophenes are studied and how these are affected by the presence of the dopants.

Chapter 2

2.1 Intrinsic properties of thermoelectric materials

When a thermoelectric material is exposed to a temperature difference, charge carriers will start moving from the hot side to the cold side leading to the formation of an electrical potential which can be used to drive current (Figure 2.1). This phenomenon, known as the Seebeck effect and initially observed by Thomas J. Seebeck in 1821, is experienced by all electrical conductors and semiconductors.[1]

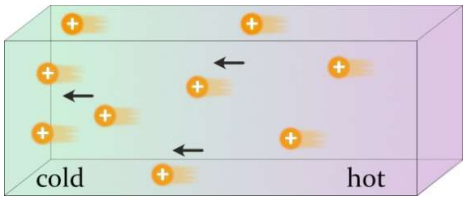

Figure 2.1. Thermoelectric effect in a p-type semiconductor.

The thermoelectric performance of a certain material is evaluated through the dimensionless figure of merit *ZT*, given by:

$$ZT = \frac{\sigma \alpha^2}{\kappa} T \tag{2.1}$$

where σ is the electrical conductivity, α is the Seebeck coefficient, and κ is the thermal conductivity of the material at a given temperature T. Therefore, a good thermoelectric material should be characterized by a high electrical conductivity σ, high Seebeck coefficient α, and low thermal conductivity κ in order to maximize *ZT*. The ideal material would embody the "phonon-glass electron-crystal" concept.[7]

The three thermoelectric parameters are unfavourably interdependent and can vary with temperature, so the optimization of the final performance requires a trade-off.

The electrical conductivity σ is proportional to the product of charge carrier concentration n and charge carrier mobility μ, given by

$$\sigma = nq\mu, \tag{2.2}$$

where q is the elementary charge, i.e. $\pm 1.6 \cdot 10^{-19}$ C. The electrical conductivity increases with the number of charge carriers, which can be modulated by doping (see Section 2.3), and with their mobility which depends on the planirity of the polymer backbone and solid-state order.

The Seebeck coefficient can be seen as a measure of the average entropy per charge carrier, so it usually decreases upon addition of charge carriers (i.e. doping). It quantifies the electrical potential ΔV that arises when a material is exposed to a temperature difference ΔT, according to $\alpha = -\Delta V/\Delta T$. The sign of the Seebeck coefficient α indicates the type of charge carriers, $\alpha < 0$ for electrons (n-type semiconductors) and $\alpha > 0$ for holes (p-type semiconductors) (Figure 2.1).

The thermal conductivity κ represents the ability of a material to transfer heat. The total thermal conductivity is composed of a lattice contribution κ_{latt} and an electronic contribution κ_e since both phonons and electrons contribute to heat transport, according to

$$\kappa = \kappa_{latt} + \kappa_e. \tag{2.3}$$

The electronic part depends on the electrical conductivity σ by the Wiedemann-Franz law $\kappa_e = L\sigma T$, where L is the Lorenz number and T is the temperature. In cases where a material has a high electrical conductivity, thermal transport is generally governed by the electronic contribution ($\kappa_e \gg \kappa_{latt}$). Conversely, materials exhibiting low electrical conductivity have a minor electronic contribution and the thermal conductivity is largely given by the phonon contribution. A phonon is a quantified lattice vibrational energy that transfers heat through lattice vibration, unless it is scattered by defects, impurities, and grain boundaries. Since polymers often possess amorphous regions and defects, their intrinsic thermal conductivity is low, and this represents one of the appealing points of using organic semiconductors for thermoelectric generators. However, the effect of introducing charge carries (i.e. doping) on the thermal conductivity κ is still unclear. Both an increase due to a larger electronic contribution[8] and a decrease due to solid-solution scattering caused by additives[9, 10] have been reported.

With all these factors combined, enhancing the figure of merit ZT is not a trivial task due to the (unfavorable) interdependency of the thermoelectric parameters. Improving one parameter could negatively impact the other. This is why the research in organic thermoelectrics

is often focused on finding an optimal point where the figure of merit ZT or the power factor $\sigma\alpha^2$ are maximized.

2.2 Conjugated polymers

Conjugated polymers are carbon-based materials that exhibit conductive or semiconductive behavior. The key feature of this class of polymers is the conjugated backbone, composed of alternating single- and double-carbon bonds (see Figure 2.2). The semiconducting nature of these polymers arises from the sp^2-hybridization of carbon bonds, i.e. a carbon atom forms both spatially localized bonds (σ-bonds) and delocalized bonds (π-bonds) with adjacent atoms.

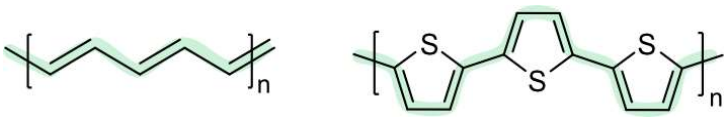

Figure 2.2. Chemical structure of conjugated polymers with the characteristic alternating single double carbon bonds.

Energy level splitting of π-bonds gives rise to bonding π- and antibonding π*-orbitals, shaping the highest occupied molecular orbital (HOMO) and the lowest unoccupied molecular orbital (LUMO), respectively. The difference in energy between HOMO and LUMO is denoted as the band gap E_g, which defines the optical and electrical properties of conjugated polymers. As the conjugation length increases, the band gap E_g decreases reaching values (< 3 eV) typical for semiconductors materials.

However, the conjugation is not enough to make the polymer electrically conductive, akin a highway without cars. Thus, the introduction of charge carriers or "cars" becomes necessary, which can be achieved through doping. Doping not only introduces charge carriers but also induces modification in the structure of the "highways" (further details in Sections 2.3 and 2.4).

2.3 Chemical doping of conjugated polymers

Chemical doping is a powerful technique for introducing charge carriers into conjugated polymers, and in turn for tailoring their electrical properties. This process involves a charge transfer between the conjugated polymer and the dopant species, resulting in the formation of

polarons, i.e. radical cations or anions, on the polymer backbone. The charge neutrality of the system is maintained by the dopant counterions.

The two most common doping mechanisms are redox doping and acid-base doping. The former entails the use of molecular dopants, which are oxidizing or reducing species. Through a redox reaction, the dopants exchange one or more electrons with the conjugated polymer, resulting in either p- (i.e. dopant accepts electrons from the polymer) or n-doping (i.e. dopant donates electrons to the polymer) (Figure 2.3).[11] Redox doping can also occur through the presence of atmospheric oxygen or water. They can act as oxidizing agents, or they can react with the dopant to first produce a radical (active compound) that subsequently undergoes charge transfer with the polymer.[12] In acid-base doping, the charge transfer takes place through the transfer of a proton (H^+) or hydride (H^-) resulting in p-doping or n-doping, respectively (Figure 2.3).[13, 14]

Generally, two methods are used for chemically doping conjugated polymers: (1) co-processing and (2) sequential processing. Co-processing involves blending conjugated polymer and dopant in the same solution and processing the resulting solution using techniques such as spin coating or drop casting. Sequential processing, instead, comprises of two steps: first processing the conjugated polymer into a solid sample and then exposing it to the dopant solution or vapor (Figure 2.3). An alternative approach is ion-exchange doping, where a conjugated polymer film is subjected to a strong oxidizing (or reducing) dopant that is dissolved in an electrolyte solution. Oxidation (or reduction) of the film is followed by exchange of the dopant counterions with different ions from the electrolyte. This removes leftover dopant ions which are potentially reactive, greatly improving stability.[15]

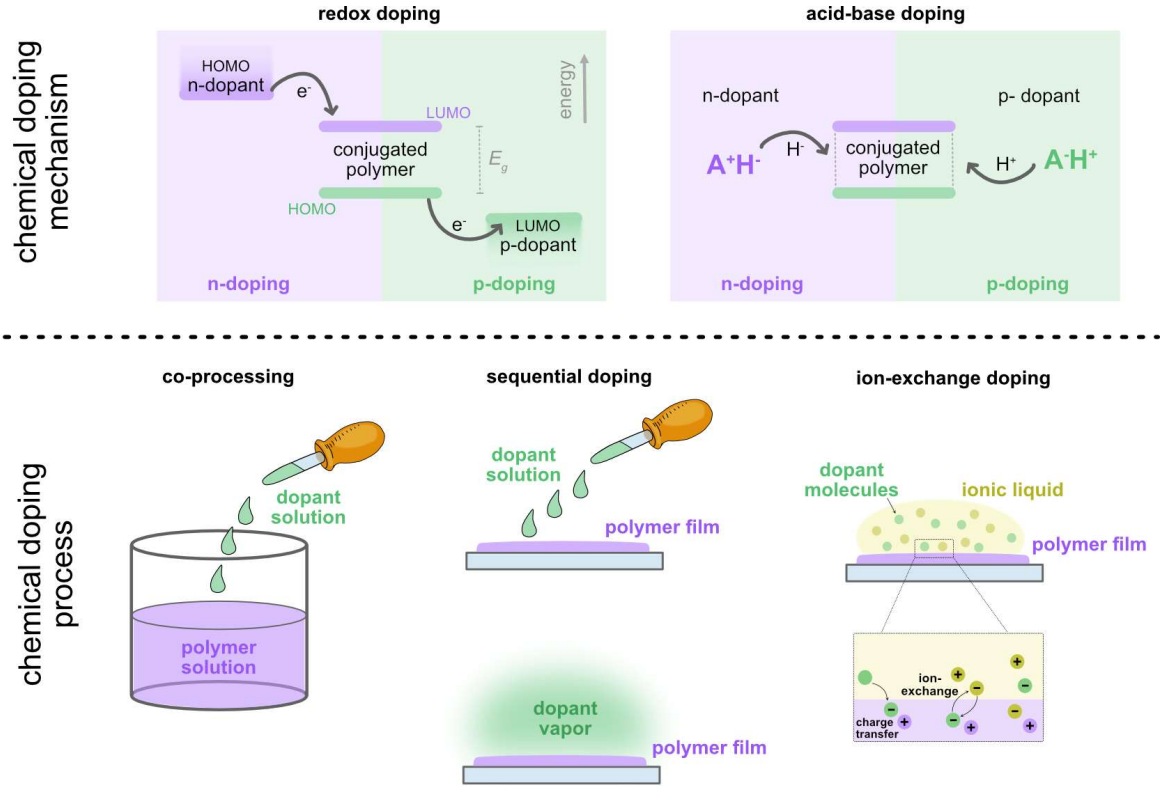

Figure 2.3. Basic principles of redox doping and acid-base doping (top); schematic of different doping processes: co-processing, sequential doping with dopant solution or dopant vapor, and ion-exchange doping.

2.4 Effect of chemical doping on solid-state order and charge transport

Doping conjugated polymers for thermoelectric applications comprises introduction of a considerable amount of dopant, i.e. tens mol % with respect to the repeat unit, in order to reach high electrical conductivities. This addition can significantly alter the nanostructure of conjugated polymers, which has a direct effect on the resulting electrical properties of the material.

Upon doping, the nano- and microstructure can be altered in terms of degree of order, crystal structure and size, and connectivity between ordered domains. A number of studies have focused on investigating how chemical doping influences the structural arrangement of various conjugated polymers, such as thiophene-, thienothiophene- and diketopyrrolopyrrole-based polymers.[16,17] However, here polythiophenes are considered, like the model poly(3-

hexylthiophene) (P3HT), which shares the identical chemical backbone structure as the polymers studied in this thesis.

Doping P3HT with the p-dopant 2,3,5,6-tetrafluoro-7,7,8,8-tetracyanoquinodimethane (F_4TCNQ) can lead to a change in the crystal structure of the polymer. The intercalation of the dopant within the crystallites of P3HT can result in a new crystalline phase characterized by larger lamellar distance.[18-20] Additionally, a reduction in the π-stacking distance can occur, which can be attributed to the side chain geometry or to the delocalization of polarons across the polymer backbone. The former can encourage closer stacking of polymer chains, while the delocalization of polarons can slightly pull together the backbones in the π-stacking direction.[21, 22]

The presence of dopant counterions, in the case of either F_4TCNQ or tris(4-bromophenyl)ammoniumyl hexachloroantimonate (known as Magic blue), into the amorphous regions of P3HT can lead to a modification of the conjugation length of the disordered polymer chains, improving the connectivity between ordered domains and leaving the structure of nanocrystals unaltered.[23, 24]

Moreover, molecular doping can induce structural reorganization within less ordered conjugated polymers, resulting in the formation of a more crystalline structure. For example, the incorporation of F_4TCNQ into regiorandom P3HT leads to an increase in both crystallinity and molecular ordering of the original structure (Figure 2.4).[25, 26] A similar effect of dopant-induced order has been observed for a polythiophene with tetra ethylene glycol side chains (p($g_4$2T-T)) doped with F_4TCNQ.[27]

The nanostructure plays a crucial role in determining the charge transport of conjugated polymers, so it is important to know how these structural changes, i.e. introducing dopants, affect the material.

To achieve efficient charge transport, charges must be able to move freely between sites without being trapped or scattered. Consequently, several factors can influence charge-carrier mobilities, including molecular packing, disorder, presence of impurities, temperature, electric field, and charge-carrier density.

For instance, within ordered domains, the delocalization of charges is enhanced by π-stacking which is facilitated by the wavefunction overlap. This phenomenon enhances the mobility of charges.[28] Conversely, structural defects, such as conformational changes that lead

to backbone twisting, amorphous domains, as well as defects in ordered domains, lead to a loss of conjugation and therefore hinder the mobility of charge carriers.[29]

Further, the connectivity between ordered domains has a pronounced effect on the charge carrier mobility. Tie chains, amorphous segments of the polymer chain that bridge adjacent crystallites, can lead to a higher charge-carrier mobility compared to polymers with high degree of order. The mobility of the latter is limited by the grain boundaries.[30]

Charge transport in molecularly doped systems is not only influenced by structural characteristics, but it also depends on several factors including Coulomb interactions between the charges and the dopant counterions, ionization efficiency and dissociation efficiency.

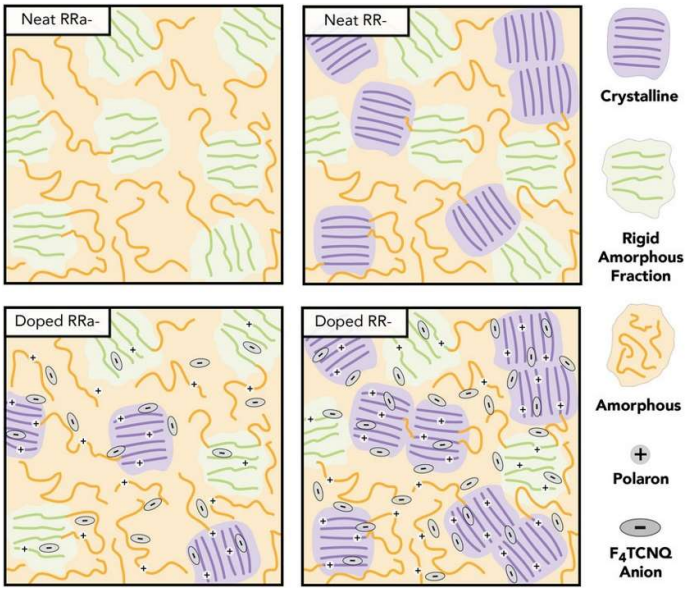

Figure 2.4. Impact on the microstructure of regiorandom (left) and regioregular (right) P3HT upon doping with F_4TCNQ. Reproduced with permission from ref. [26] published by WILEY 2019.

2.5 Effect of chemical doping on mechanical properties

Mechanical flexibility and robustness are two desired characteristics for organic thermoelectric generators, in order to implement them in wearable technologies and IoT applications (Chapter 1.2). Therefore, the investigation of the mechanical properties of conjugated polymers becomes crucial to assess their suitability for the design of future devices.

The mechanical properties and the viscoelastic behavior of polymers are significantly determined by their nano- and microstructures. For instance, conjugated polymers with a low degree of crystallinity, such as polythiophenes with oligoether side chains, tend to be soft at room temperature, with a glass transition temperature T_g below 0 °C.[27, 31] The T_g is the temperature associated to a transition from the glassy to the rubbery state of the material due to the onset of main-chain relaxation and it usually determines the mechanical properties around room temperature. On the other side, regio-random poly(3-butylthiophene) (P3BT) characterized by an high degree of order displays a $T_g \approx 45$ °C, being in the glassy state at room temperature with a shear storage modulus of about 700 MPa.[32]

Doping can strongly alter the nano- and microstructure of conjugated polymers (Section 2.4) and these alterations can be directly translated into a modification of their mechanical properties through different effects including plasticization, a change in the degree of order and a change in T_g. Indeed, chemical doping has been recently reported as 'a tool to not only control the electrical but also mechanical properties of conjugated polymers' by Zokaei *et al* [27].

The presence of dopant counterions into the lamella structures of semicrystalline conjugated polymers can induce a plasticization effect by reducing the interchain interactions. For example, regioregular (95%) P3HT when doped with ethylbenzene sulfonic acid (EBSA) undergoes to a plasticization effect, showing a decrease in T_g from 30 to 15 °C and in elastic modulus from 900 to 345 MPa (Figure 2.5).[33] A similar effect occurs in free-standing and tensile-drawn films of P3HT when doped with the molybdenum dithiolene complex Mo(tfd-$COCF_3$)$_3$, yielding a reduction in elastic modulus from 1.1 GPa to 0.4 GPa.[34] Likewise, highly stiff poly(2,5-dimethoxy-p-phenylenevinylene) (PDMPV) fibers experience a reduction in elastic modulus from 35 GPa to 25 GPa when doped with iodine (Figure 2.5).[35]

In contrast to the plasticization effect, chemical doping can increase the material stiffness by enhancing the π-stacking and degree of order. This effect has been observed especially in softer conjugated polymers. For instance, p($g_4$2T-T) with elastic modulus of 8 MPa at room temperature, can experience a 29-fold increase in modulus, up to 232 MPa, along with a change in T_g from -43 to 3 °C, when doped with 30 mol% F_4TCNQ (Figure 2.5).[27]

Both electrical and mechanical properties of conjugated polymers are significantly influenced by their nano- and microstructure, leading to interdependencies between them. The presence of ordered domains, which can be crystallites or regions where π-stacking occurs, concomitantly enhances charge transport and increases the elastic modulus.[36]

Another element that establishes a correlation between electrical and mechanical properties are tie chains, which connect ordered domains in conjugated polymers with sufficiently high molecular weight. Tie chains lead to an increase in charge-carrier mobility due to an improved connectivity between ordered domains, and at the same time they contribute to the ductility of the material, allowing it to deform at larger elongations without undergoing breakage.

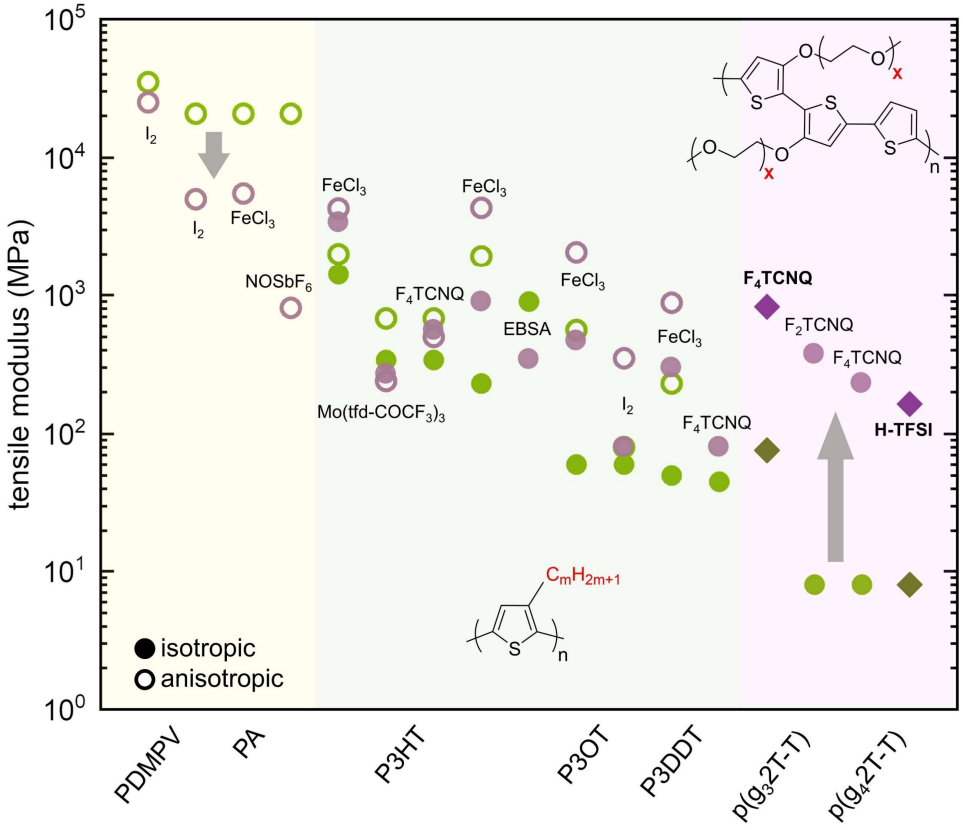

Figure 2.5. Impact of chemical doping on the tensile elastic modulus of PDMPV, PA and various polythiophenes with alkyl and oligoether side chains. Green symbols represent the conjugated polymer in its neat state, while purple symbols are doped polymers; diamond symbols represent data from this thesis, circle symbols are data from [27, 33-40]. Adapted from ref. [41].

Chapter 3

EXPERIMENTAL

This chapter presents the materials and characterization techniques chosen in this thesis for investigating the effect of chemical doping on thin films and bulk samples.

3.1 Materials

3.1.1 Polythiophenes with oligoether side chains

Unsubstituted conjugated polymers such as polythiophene, polyaniline and PEDOT tend to be intractable. One common tool to impart processability is the decoration of the backbone with solubilizing side chains. In particular, the presence of oligoether side chains improves the solubility of the polymer in polar solvents, thus rendering it compatible with solution-based processing. It has been shown that using polar side chains instead of alkyl side chains enhances the compatibility between dopant and host polymer.[14, 42] Moreover, the presence of oligoether side chains seems to lead to an overall increase in the dielectric constant of the material, resulting in higher charge-carrier mobility.[43]

In this thesis, three oligoether-substituted polythiophenes with different side-chain length are studied. The repeat unit of the polymers is g_x2T-T and the side chains comprise 3, 4 or 6 units of ethylene glycol, herein referred to as p(g_x2T-T) (see Figure 3.1). p($g_4$2T-T) was synthetized by Dr. Renee Kroon according to ref. [42] (**paper I** and **paper II**), while p($g_3$2T-T) and p($g_6$2T-T) were synthetized by Sophie Griggs and Junfu Tian according to ref. [44] (**paper II**).

3.1.2 Dopants

This thesis focuses on two different doping mechanism: oxygen-mediated acid doping (**paper I**) and redox doping (**paper II**). Bistriflimidic acid (H-TFSI) is used as acid dopant, which is an effective dopant for p($g_4$2T-T) as reported in previous studies.[13] The common p-dopant F_4TCNQ with an electron affinity (EA) of around 5.2 eV[45] is selected as oxidizing

species for redox doping (Figure 3.1) since the ionization energy (IE) of the polymers is around 4.5 eV.[44]

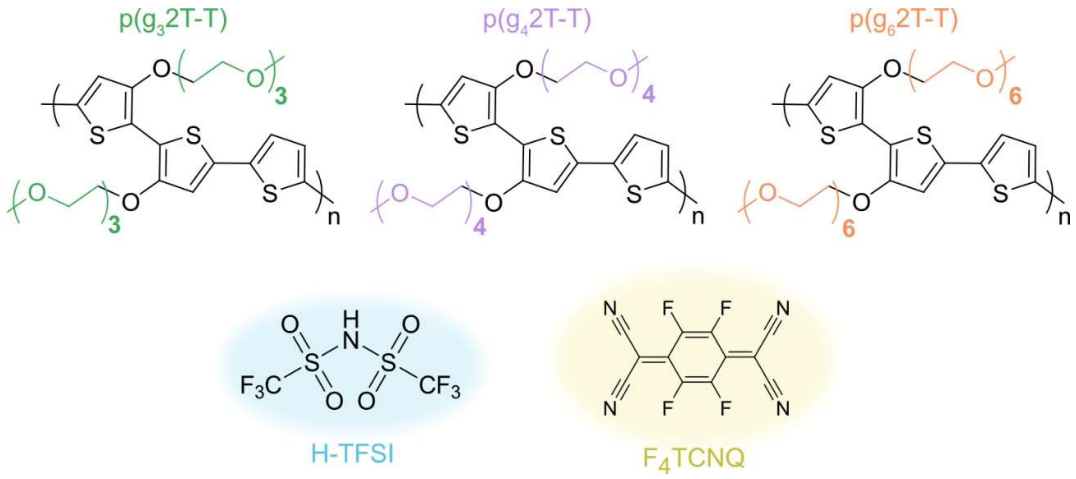

Figure 3.1. Chemical structure of oligoether-substituted polythiophenes and dopants used in this thesis.

3.2 Sample preparation and doping

In this thesis, the co-processing method of doping is studied (Figure 2.3).

In **paper I**, p($g_4$2T-T) was dissolved at 6 g L^{-1} in a mixture of chloroform ($CHCl_3$) and anhydrous acetonitrile (AcN) (3:2, v:v), while H-TFSI was dissolved at 10 g L^{-1} in anhydrous acetonitrile. Appropriate amounts of these two solutions were mixed to prepare solutions containing different amounts of H-TFSI (4, 7, 10, 18, 25 and 40 mol%) and p($g_4$2T-T). The molar percentage of H-TFSI is calculated with respect to the number of thiophene rings per repeat unit of the polymer.

In **paper II**, p($g_3$2T-T), p($g_4$2T-T) or p($g_6$2T-T) were dissolved at 4 g L^{-1} in $CHCl_3$ and F_4TCNQ in AcN (2 g L^{-1}). The polymer and dopant solutions were mixed in order to obtain a dopant concentration of 20 mol%, and a further addition of AcN or $CHCl_3$ to ensure a final solvent ratio of 2:1 $CHCl_3$:AcN was made. The molar percentage of F_4TCNQ was calculated with respect to the number of thiophene rings per repeat unit of the polymer.

The polymer:dopant solutions were subsequently bar-coated or spin-coated onto substrates (glass, PET, silicon) for thin films preparation. Free-standing films were prepared by drop-casting the solutions onto the substrate or glass mesh strands.

3.3 Characterization of thin samples

3.3.1 Structural order

Grazing Incidence Wide-Angle X-ray Scattering (GIWAXS) was employed to examine the molecular-level structural organization of p(g_x2T-T) polymers via X-ray diffraction. This diffraction technique enables the investigation of sample surfaces or extremely thin films by utilizing an X-ray beam that approaches the sample surface at a nearly horizontal angle.

3.3.2 Optoelectronic and thermoelectric properties

UV-vis spectroscopy serves as a method for characterizing electronic transitions within thin polymer films. Polymers featuring π-electrons can absorb light energy in the UV-vis-NIR (ultraviolet-visible-near infrared) range, thereby exciting these electrons to higher anti-bonding π-molecular orbitals.

The main optical absorption of the undoped polymers undergoes a substantial red-shift after doping, owing to the formation of polaronic levels. New absorption peak in the long-wavelength region (NIR) will appear at the same time, which demonstrates the doping process.

The electrical resistivity was measured using a four-point probe setup with co-linear tungsten carbide electrodes which has the advantage of eliminating possible contact resistance. In this configuration, a current is forced on the two outer electrodes and the voltage is measured on the two inner electrodes. The sheet resistance $R_s = {}^{\pi}/_{ln2} \cdot {}^{V}/_{I}$ was then calculated and the obtained value was used to determine the electrical conductivity according to $\sigma = {}^{1}/_{(R_s \cdot t)}$ where t is the sample thickness.

The Seebeck coefficient of the doped samples was measured by recording the voltage change when the material is subjected to a temperature gradient. A ~ 5 mm long sample was mounted onto a sample holder that also holds a Constantan reference, whose Seebeck coefficient is well known. Both the sample and the reference were exposed to the same thermal

gradient conditions. The voltage change observed across the sample, in comparison to the reference, is directly linked to the difference in Seebeck coefficients between the sample and the reference material.

3.4 Characterization of free-standing samples

3.4.1 T_g measurements

Calorimetry and thermodynamic analysis were used to determine the glass transition temperature T_g of the polymers. In **paper I**, the T_g was measured by differential scanning calorimetry (DSC), a method that records the thermal energy (heat) as a function of temperature or time. Instead, a dynamic mechanical analyzer (DMA), which determines the viscoelasticity of polymers as a function of temperature or time, was used in **paper II**. By applying a sinusoidal strain within the elastic regime while performing a temperature ramp allows to determine the glass transition temperature of polymers.

3.4.2 Mechanical properties

Tensile testing was performed on free standing films by using a DMA in tensile mode (Figure 3.2). It was used to determine the stiffness, elasticity, and stretchability of the polymers in their neat and doped states. During the test, the sample was deformed in one direction at constant force rate (force-controlled mode), which allowed to record the stress as a function of strain until fracture.

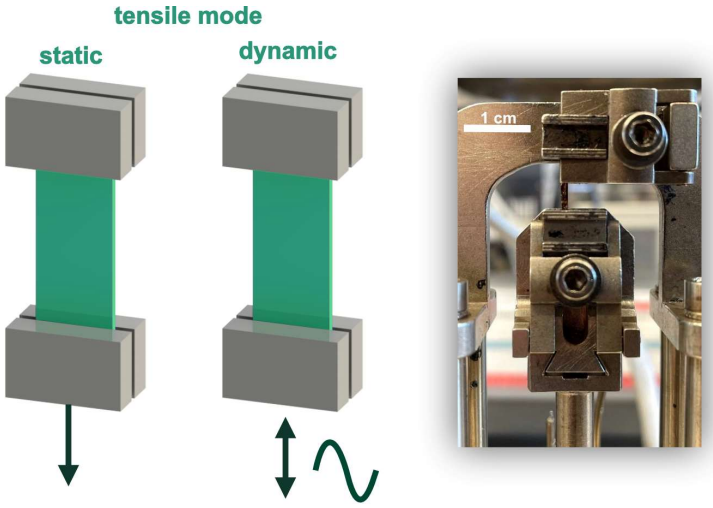

Figure 3.2. Schematic of the working principles of DMA in static or dynamic mode. A picture of a free-standing sample mounted in the DMA clamps.

Chapter 4

RESULTS

As discussed in Sections 2.4 and 2.5, the thermoelectric and mechanical properties of conjugated polymers are strongly connected to their nano- and microstructure. This chapter presents and discusses the results of the investigation about the impact of chemical doping polar polythiophenes on their degree of order and, consequently, on their thermoelectric performance. Furthermore, the change in the thermomechanical properties of these polythiophenes upon chemical doping is presented and discussed.

4.1 Impact of chemical doping on the structural and thermoelectric properties of thin films

Grazing-incidence wide-angle X-ray scattering was used to determine the degree of order of the three polymers, p($g_3$2T-T), p($g_4$2T-T) and p($g_6$2T-T), in their neat and oxidized states in order to investigate how the length of side chains and the presence of dopant can affect the microstructure.

All three neat polymers show a low degree of order with out-of-plane $h00$ diffraction peaks, which indicate the lamella stacking, at $q_{100} \approx 0.30$ Å^{-1} for p($g_3$2T-T) and $q_{100} \approx 0.35$ Å^{-1} for p($g_4$2T-T) typical for an edge-on texture of the polymer backbone (Figure 4.1). A weak in-plane q_{010} diffraction, which represents the π-stacking, is observed for p($g_3$2T-T), indicating limited π-stacking, on top of a broad amorphous halo at $q \approx 1.5$ Å^{-1}; while no q_{010} can be discerned for p($g_4$2T-T) and p($g_6$2T-T).

Doping with either H-TFSI or F_4TCNQ results in a change in texture from a predominately edge-on to face-on orientation, as evidenced by in-plane $h00$ diffraction peaks and by a clear out-of-plane diffraction peak $q_{010} \approx 1.75$ Å^{-1} that emerges due to π-stacking of the polymer backbone. This indicates that the presence of dopant counterions induces an increase of structural order of the polymers, like in the case of doped regiorandom P3HT.[25]

By comparing the out-of-plane q_{010} diffraction peak of p(g_x2T-T) polymers co-processed with 20 mol% of F_4TCNQ (**paper II**), a decrease in intensity with increasing side-chain length is observed (Figure 4.1c), indicating a higher degree of order for the polymer with the shortest side chains, i.e. p($g_3$2T-T).

Further, the degree of order is affected not only by the side-chains length, but also by the amount of dopant introduced (**paper I**). Indeed, upon the addition of up to 7 mol% H-TFSI to p($g_4$2T-T) the intensity of the diffraction peak indicating π-stacking increases, and then decreases together with a shift to lower q values at higher H-TFSI concentrations (Figure 4.1a). Interestingly, p($g_4$2T-T) films that contain a large amount of H-TFSI (25 and 40 mol%) give rise to GIWAXS diffractograms that are more comparable to neat p($g_4$2T-T) with an out-of-plane q_{100} diffraction and a weak q_{010} diffraction. Therefore, the degree of π stacking also depends on the amount of dopant counterions present in the sample, in particular it is favored at low dopant concentrations, while it is hindered at high dopant concentrations. A lower degree of order at high dopant concentrations may indicate that polaron/counterion interactions reduce the ability of the polymer to order.

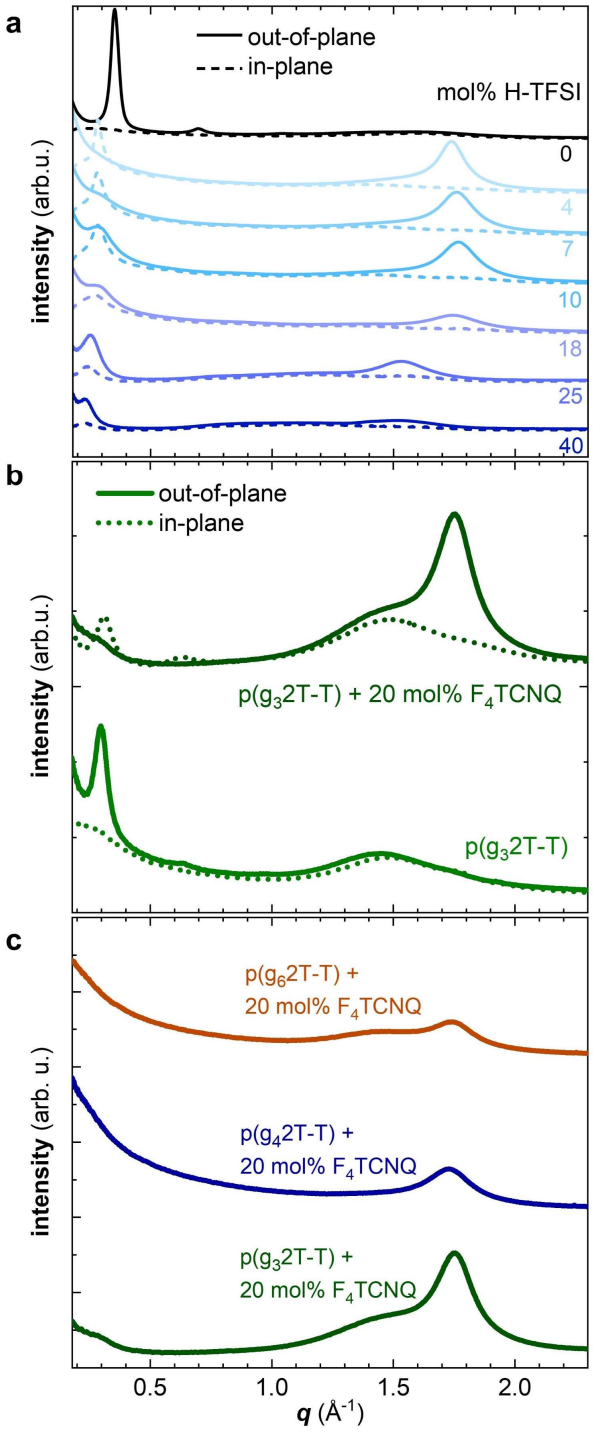

Figure 4.1. GIWAXS diffractograms of p($g_4$2T-T) co-processed with different amounts of H-TFSI (a), p($g_3$2T-T) co-processed with 20 mol% of F_4TCNQ (b), and p(g_x2T-T) co-processed with 20 mol% of F_4TCNQ (c).

The degree of solid-state order strongly impacts the charge transport properties of conjugated polymers, as discussed in Section 2.4. Therefore, we measured the thermoelectric properties of all the polymer:dopant systems to investigate how they are affected by the sample microstructure.

Acid doping p(g$_4$2T-T) with H-TFSI (**paper I**) results in an increase of the electrical conductivity σ together with a decrease in the Seebeck coefficient α. In particular, the electrical conductivity increases with the dopant concentration up to 25 mol% H-TFSI, where it reaches a conductivity of ~ 20 S cm^{-1}, followed by a decrease to ~ 5 S cm^{-1} for higher H-TFSI mol% values (Figure 4.2). The electrical conductivity decreases as dopant amount reaches 40 mol% H-TFSI despite a further increase in the oxidation level, as evidenced by UV-vis spectroscopy (Figure 4.2), suggesting that the electrical conductivity is limited by a reduction in the charge-carrier mobility due to a lower degree of order (Figure 4.1).

Interestingly, p(g$_4$2T-T) films co-processed with H-TFSI and aged for 2 days at ambient conditions exhibit a higher electrical conductivity compared to the initial as-cast films, with the highest value equal to 58 S cm^{-1} at 25 mol% H-TFSI. Similar values of electrical conductivity were reported by Hofmann *et al.*,[13] indicating that ageing for 2 days was sufficient for the thin films to reach a steady state. The observation that a high electrical conductivity is only obtained when the material is exposed to air can be explained by considering the role of O_2 in the doping mechanism. Indeed, acid doping of p(g$_4$2T-T) can lead to protonation of the backbone, but it may also promote an acid-mediated oxidation of the polymer through O_2.[46]

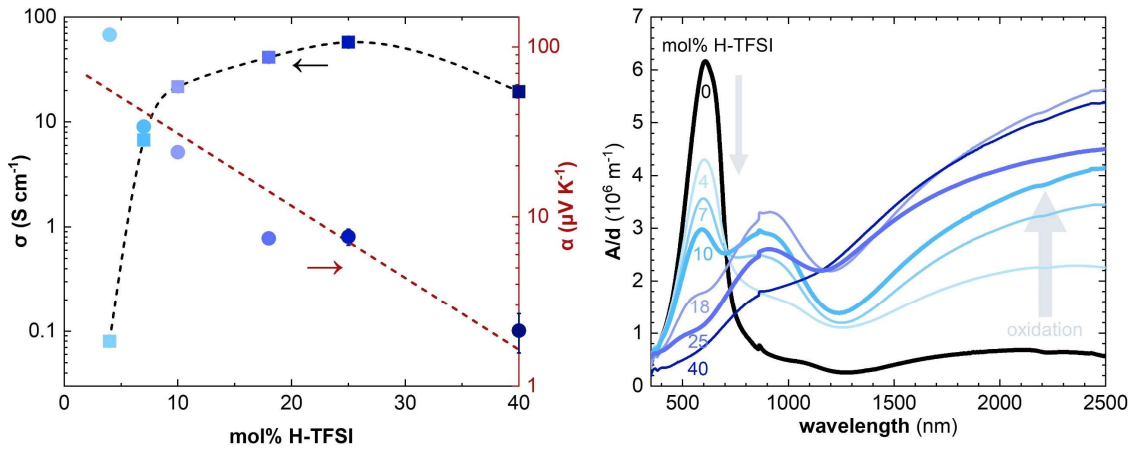

Figure 4.2. Thermoelectric properties, i.e. electrical conductivity σ and Seebeck coefficient α, and UV-vis absorption spectra of p(g$_4$2T-T) co-processed with different amounts of H-TFSI.

In **paper II**, the impact of the side-chain length on thermoelectric properties of p(g_x2T-T) co-processed with the same dopant concentration, i.e. 20 mol% F_4TCNQ, was investigated and a significant influence of the side-chain length is observed. P($g_3$2T-T) displays the highest electrical conductivity among the three analyzed polymers, reaching a value of σ = 830 ± 15 S cm^{-1} (Table 4.1, Figure 4.3). Instead, p($g_4$2T-T) and p($g_6$2T-T) show comparable values of σ = 56 ± 3 S cm^{-1} and 51 ± 4 S cm^{-1}, respectively.

By analyzing the UV-vis spectra of doped films, the number of charge carriers, i.e. polarons, N_p^{UVvis} per unit volume, was estimated. This allowed to determine the charge-carrier mobility μ according to Equation 2.2. P($g_3$2T-T) exhibits the highest charge-carrier mobility μ = 18.7 ± 5.6 cm^2 V^{-1} s^{-1}, which is one order of magnitude larger than values obtained for the other two polymers. This aligns with the higher degree of order and more pronounced π-stacking of p($g_3$2T-T) compared to p($g_4$2T-T) and p($g_6$2T-T).

Table 4.1. Electrical properties of thin films co-processed with 20 mol% F_4TCNQ per thiophene ring: polymer, ionization efficiency η_{ion}^{UVvis} and number of polarons per unit volume N_p^{UVvis} from analysis of UV-vis spectra (estimated error of 30% based on uncertainty in thickness measurement and the analysis of UV-vis spectra), electrical conductivity σ (error represents the standard deviation of five measurements on the same sample), charge mobility μ, Seebeck coefficient α (error represents the standard deviation of five measurements on the same sample), and power factor $\alpha^2\sigma$.

polymer	η_{ion}^{UVvis} (%)	N_p^{UVvis} (10^{26} m^{-3})	σ (S cm^{-1})	μ (cm^2 V^{-1} s^{-1})	α (μV K^{-1})	$\alpha^2\sigma$ (μW m^{-1} K^{-2})
p($g_3$2T-T)	42 ± 14	2.8 ± 0.8	830 ± 15	18.7 ± 5.6	15.8 ± 2.0	20.7 ± 3.8
p($g_4$2T-T)	36 ± 12	2.1 ± 0.6	56 ± 3	1.7 ± 0.5	13.8 ± 0.5	1.1 ± 0.1
p($g_6$2T-T)	28 ± 9	1.4 ± 0.4	51 ± 4	2.3 ± 0.7	14.1 ± 0.7	1.0 ± 0.1

Conversely to the electrical conductivity, the Seebeck coefficient does not show a dependence from the side-chain length. Values for all three polymers are similar, around α = 14 to 16 μV K^{-1}.

We monitored the thermoelectric properties over time to study the stability of 20 mol% F_4TCNQ-co-processed p($g_3$2T-T) polymer at ambient conditions (Figures 4.3). The doped polymer is sensitive to air, as evidenced by a drop in electrical conductivity within the first 24 hours of aging, thus leading to a decrease in the thermoelectric performance. After an initial drop in σ, the thermoelectric properties display a promising level of long-term stability.

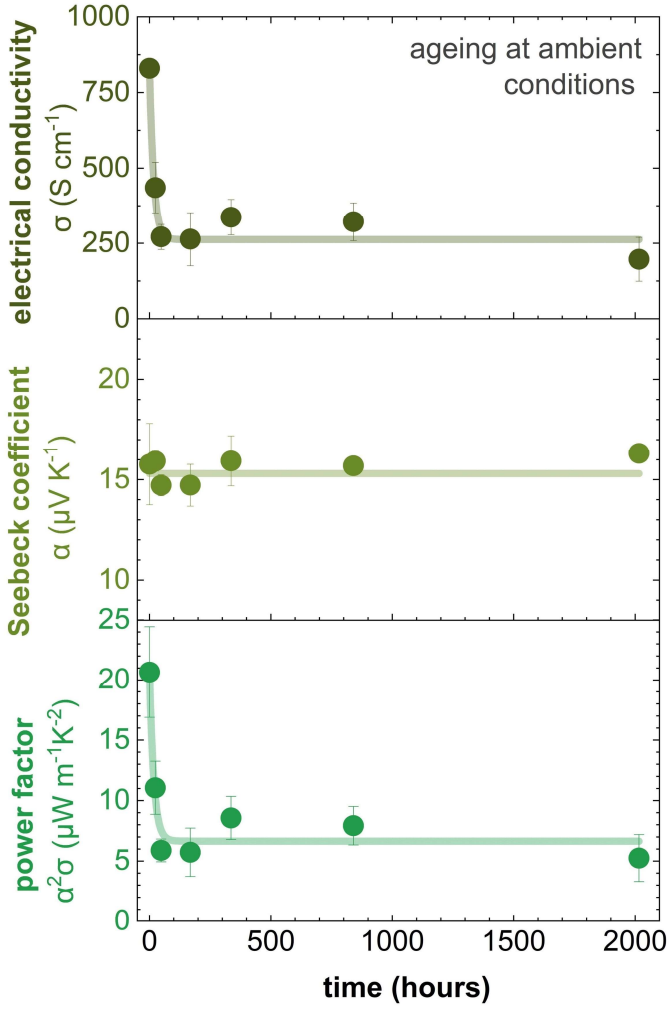

Figure 4.3. Electrical conductivity, Seebeck coefficient and power factor vs ageing time of p($g_3$2T-T) co-processed with 20 mol% of F_4TCNQ at ambient conditions.

4.2 Impact of chemical doping on the thermomechanical properties of free-standing samples

The investigation of mechanical properties of conjugated polymers is fundamental to assess their suitability for the design of organic thermoelectric generators.

The glass transition temperature of the neat p(g_x2T-T) polymers was first measured. In **paper II**, the effect of side-chain length on T_g was investigated by recording the change in tensile modulus as a function of temperature of neat p(g_x2T-T) supported by a glass fiber mesh through dynamic mechanical analysis (DMA). The DMA thermographs (Figure 4.4) reveal a similar T_g, which corresponds to the peak in the loss modulus E'', of -36 °C, -41 °C and -43 °C for side-chain length equal to 3, 4, and 6 ethylene glycol repeat units, respectively. Similar to poly(3-alkylthiophene)s (P3ATs) featuring long alkyl side chains (e.g. decyl, dodecyl), an increase in the side-chain length from triethylene glycol to tetra- or hexaethylene glycol only slight reduces the T_g.[47]

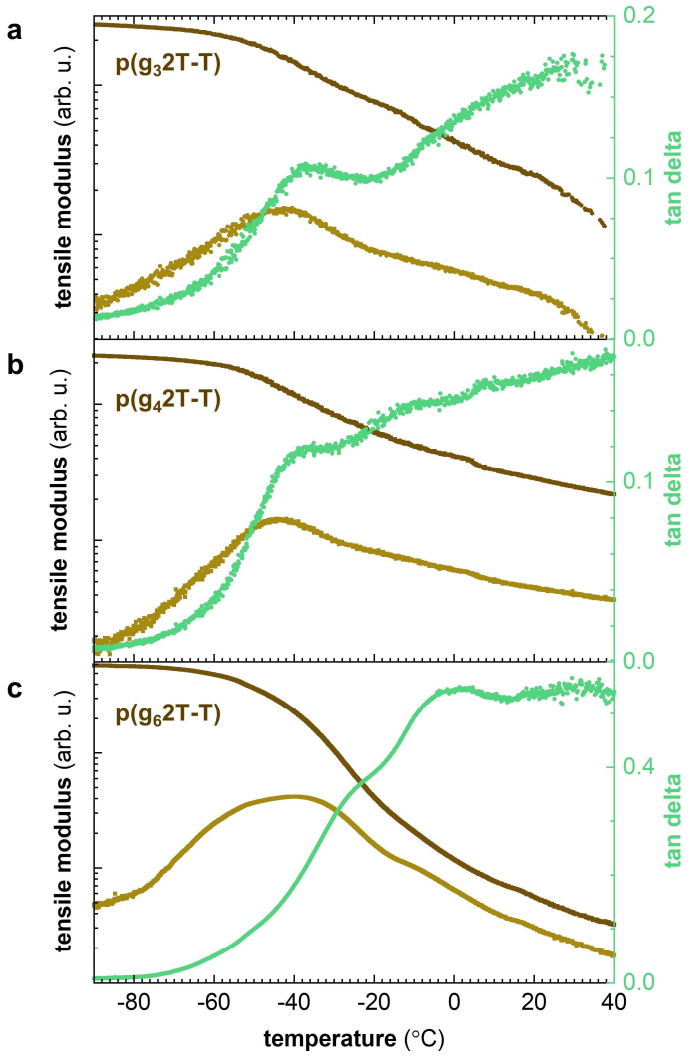

Figure 4.4. Tensile storage *E'* (dark brown) and loss (light brown) modulus E'', and $tan\delta = E''/E'$ (green) of neat p($g_3$2T-T) (a), p($g_4$2T-T) (b) and p($g_6$2T-T) (c) recorded as a function of temperature on samples supported by a glass fiber mesh.

Co-processing p(g_x2T-T) with 20 mol% F_4TCNQ considerably increases the T_g from -36 °C to 1 °C in the case of p($g_3$2T-T) (Figure 4.5) and from - 41 °C to 3 °C in the case of p($g_4$2T-T) as reported by ref. [27]. The increase in T_g can be explained with the doping-induced π-stacking of the polymer (Section 4.1), and with a change in the rigidity of the backbone upon oxidation. The T_g of doped polymers was measured using free-standing samples, and this limited the measurement of p($g_6$2T-T) co-processed with 20 mol% F_4TCNQ.

Chemically doping p(g$_4$2T-T) with H-TFSI (**paper I**) leads to a similar effect. The change in T_g of p(g$_4$2T-T) co-processed with different amounts of H-TFSI was studied by differential scanning calorimetry (DSC) at a scan rate of 10 °C min^{-1}. The T_g increases with mol% of H-TFSI, reaching the highest value of -32 °C (starting from -59 °C of the neat polymer) for aged material doped with 40 mol% H-TFSI (Figure 4.5). The increase in T_g observed in p(g$_4$2T-T) when co-processed with H-TFSI is less pronounced compared to the increase achieved through doping with F$_4$TCNQ (Figure 4.5). This difference is thought to be due to changes in the conformation of the polymer, possibly due to protonation in case of doping with H-TFSI, as well as the location of the anion relative to the polymer backbone. Indeed, as suggested by MD simulations, TFSI anions are positioned further away from the polymer backbone than F$_4$TCNQ anions. The difference in the T_g of doped polymers suggests that molecular dopants and acid dopants can yield different outcomes with regard to the mechanical properties, with the latter potentially inducing a more pronounced plasticization effect.

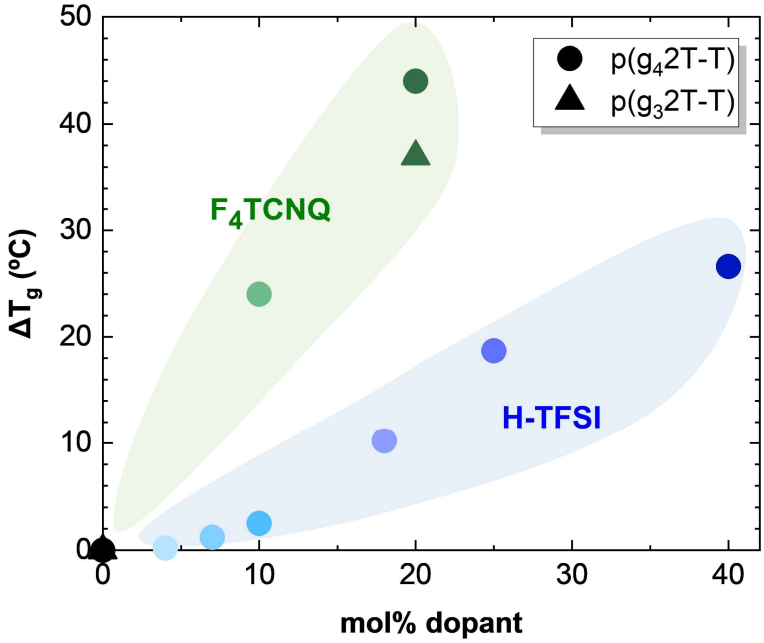

Figure 4.5. Glass transition temperature difference ΔT_g vs. dopant concentration of p(g$_3$2T-T) and p(g$_4$2T-T) doped with H-TFSI or F$_4$TCNQ. The ΔT_g is calculated according to $T_{g,doped} - T_{g,neat}$, where $T_{g,neat}$ is -36 °C for p(g$_3$2T-T) (measured by DMA), -41 °C for p(g$_4$2T-T) (measured by DMA), and -59 °C for p(g$_4$2T-T) (measured by DSC).

In the last set of experiments, we used tensile deformation of free-standing samples at room temperature to analyze the stiffness and elongation at break of neat and doped polymers (Figure 4.6).

A correlation between side-chain length and resultant stiffness and stretchability of the materials is found. Indeed, shortening the length of side chains enhances the stiffness of the polymer, as indicated by the Young's modulus of 76 MPa for neat p($g_3$2T-T) and of 8 MPa for p($g_4$2T-T), and significantly reduces the stretchability.[27] A similar effect of side-chain length was also observed for P3ATs.[36]

Upon co-processing with dopants, both with F_4TCNQ or H-TFSI, the polymers become stiffer. In the case of p($g_3$2T-T) doped with 20 mol% F_4TCNQ (**paper II**), the Young's modulus increases by a factor of 10, reaching a value of E = 826 ± 141 MPa, while maintaining a similar elongation at break. Similarly, the elastic modulus of p($g_4$2T-T) co-processed with H-TFSI (**paper I**) increases up to (164 ± 11) MPa at 18 mol% H-TFSI, i.e. 8-fold higher than the modulus of the undoped material. This observed change in stiffness upon doping aligns with the higher degree of order induced by chemical doping. So, the presence of ordered domains is expected to benefit charge transport and to increase the Young's modulus of the material, confirming the correlation between electrical and mechanical properties. However, at high H-TFSI concentrations (25 and 40 mol%) the elastic modulus decreases.

Moreover, it is interesting that p($g_4$2T-T) samples co-processed with 10 mol% and 25 mol% of H-TFSI show similar elastic moduli but different electrical properties. This indicates that in some cases the mechanical and electrical properties are not coupled.

The change in mechanical properties upon doping confirms that chemical doping can be used as tool not only for adjusting the electrical properties but also for tuning the mechanical properties of conjugated polymers.

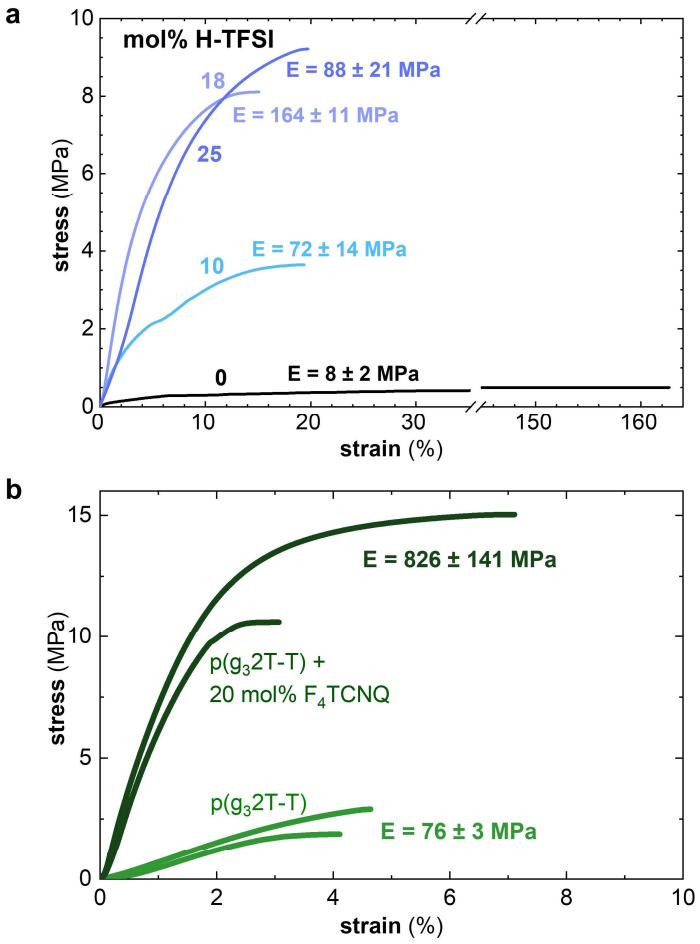

Figure 4.6. Stress-strain curves recorded by tensile deformation of: (a) p($g_4$2T-T) neat and co-processed with different amounts of H-TFSI, and (b) p($g_3$2T-T) neat (light green) and co-processed with 20 mol% of F_4TCNQ (dark green).

Chapter 5

CONCLUSIONS AND OUTLOOK

5.1 Conclusions

In this thesis, structure-property relationships with regard to thermoelectric properties of p-doped oligoether substituted polythiophenes were studied. In particular, the importance of solid-state order of conjugated polymers for improving their charge transport properties and for tuning their mechanical properties was demonstrated.

Varying the length of oligoether side chains influenced the resulting degree of order of the polymer films. Notably, the polymer having the shortest side chains, i.e. p($g_3$2T-T), exhibited the highest degree of structural order, whether in its pristine or oxidized states, among the three analyzed polymers. This directly translated to higher thermoelectric properties, primarily attributed to the enhanced charge-carrier mobility, and thus electrical conductivity, favored by more pronounced π-stacking.

Furthermore, chemical doping induced an ordering effect in the polymers. Doping the p(g_x2T-T) polymer series with either F_4TCNQ or H-TFSI led to an increase of π-stacking, likely promoting the delocalization of charge-carriers. As a result, samples showing more pronounced π-stacking displayed higher electrical conductivity values. Instead, a large dopant concentration hindered the formation of structural order as confirmed by a lower electrical conductivity.

Next, the degree of order achieved through chemical doping and through the reduction of the side-chain length was correlated with the mechanical properties of the polymers. The side-chain length showed to have an impact on stiffness and stretchability of the polymers. Indeed, a short side-chain length corresponded to a stiff and less stretchable material. Similarly, the high degree of π-stacking achieved through chemical doping resulted in an increase of the glass transition temperature T_g and in a significantly higher stiffness.

However, the degree to which these changes in mechanical properties occurred varied with the type of dopant. The acid dopant H-TFSI was found to induce a higher plasticization effect than F_4TCNQ (Figure 5.1).

It was shown that the electrical and mechanical properties of conjugated polymers such as the electrical conductivity and elastic modulus tend to correlate, but they can be partially decoupled through the selection of suitable dopants.

5.2 Outlook

In future research, the aim is to expand the investigation of the effect of chemical doping on soft conjugated polymers for thermoelectric applications. Some possibilities will be to study other conjugated polymers having a different chemical structure of the backbone, as well as to investigate other processing techniques that help to increase the solid-state order of polymers, such as rubbing, tensile-drawing or fiber-spinning.

Additionally, alternative acid dopants will be explored to further elucidate the plasticization effect. By exploring a broader spectrum of polymer:dopant systems, the objective is to obtain highly conductive materials characterized by mechanical robustness and stretchability (Figure 5.1), in order to aid the selection of promising candidates for thermoelectric applications.

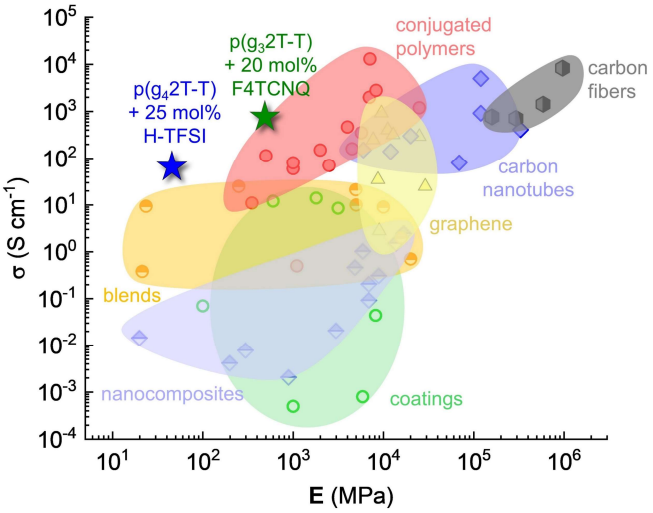

Figure 5.1. Ashby plot of the electrical conductivity vs. Young's modulus of anisotropic samples based on organic and organic-inorganic materials. References are found in ref. [48], graph is adapted from ref. [48] with permission from Elsevier 2018. Star symbols represent polymer:dopant systems studied in this thesis.

ACKNOWLEDGMENTS

I would like to thank my supervisor Christian for being a great supervisor, always taking time to discuss and guide me during the ups and downs of these two years.

Big thanks go to Joost for the fruitful discussions, for being always ready to help and for all the fun trips we had (and more to come). I owe you many columns (apparently)!

All the members of Müller's group: you are a fantastic group, thank you!
Thanks to all friends and colleagues on floor 8th for creating an incredibly friendly and positive working environment. Special thanks to Lotta for taking care of everyone.

A big thank you for the unconditional love and support that I received from my parents, my family and Ale, I would not have made it here without you!

BIBLIOGRAPHY

1. D. Beretta, N. Neophytou, J. M. Hodges, M. G. Kanatzidis, D. Narducci, M. Martin-Gonzalez, M. Beekman, B. Balke, G. Cerretti, W. Tremel, A. Zevalkink, A. I. Hofmann, C. Müller, B. Dörling, M. Campoy-Quiles and M. Caironi, *Materials Science and Engineering: R: Reports*, 2019, **138**, 100501.
2. B. Orr, A. Akbarzadeh, M. Mochizuki and R. Singh, *Applied Thermal Engineering*, 2016, **101**, 490-495.
3. H. Kaibe, K. Makino, T. Kajihara, S. Fujimoto and H. Hachiuma, *AIP Conference Proceedings*, 2012, **1449**, 524-527.
4. P. Alegría, L. Catalán, M. Araiz, Á. Casi and D. Astrain, *Geothermics*, 2023, **110**, 102677.
5. N. Pataki, P. Rossi and M. Caironi, *Applied Physics Letters*, 2022, **121**.
6. B. Dörling, J. D. Ryan, J. D. Craddock, A. Sorrentino, A. E. Basaty, A. Gomez, M. Garriga, E. Pereiro, J. E. Anthony, M. C. Weisenberger, A. R. Goñi, C. Müller and M. Campoy-Quiles, *Advanced Materials*, 2016, **28**, 2782-2789.
7. J. Liu, B. van der Zee, R. Alessandri, S. Sami, J. Dong, M. I. Nugraha, A. J. Barker, S. Rousseva, L. Qiu, X. Qiu, N. Klasen, R. C. Chiechi, D. Baran, M. Caironi, T. D. Anthopoulos, G. Portale, R. W. A. Havenith, S. J. Marrink, J. C. Hummelen and L. J. A. Koster, *Nature Communications*, 2020, **11**, 5694.
8. D. Moses and A. Denenstein, *Physical Review B*, 1984, **30**, 2090-2097.
9. O. Zapata-Arteaga, A. Perevedentsev, S. Marina, J. Martin, J. S. Reparaz and M. Campoy-Quiles, *ACS Energy Letters*, 2020, **5**, 2972-2978.
10. H. Zhao, N. Prine, G. Ma, Y. Zhang, M. A. Haque, D. Baran and X. Gu, *Sustainable Energy & Fuels*, 2023, **7**, 369-380.
11. A. D. Scaccabarozzi, A. Basu, F. Aniés, J. Liu, O. Zapata-Arteaga, R. Warren, Y. Firdaus, M. I. Nugraha, Y. Lin, M. Campoy-Quiles, N. Koch, C. Müller, L. Tsetseris, M. Heeney and T. D. Anthopoulos, *Chemical Reviews*, 2022, **122**, 4420-4492.
12. B. Yurash, D. X. Cao, V. V. Brus, D. Leifert, M. Wang, A. Dixon, M. Seifrid, A. E. Mansour, D. Lungwitz, T. Liu, P. J. Santiago, K. R. Graham, N. Koch, G. C. Bazan and T.-Q. Nguyen, *Nature Materials*, 2019, **18**, 1327-1334.
13. A. I. Hofmann, R. Kroon, L. Yu and C. Müller, *Journal of Materials Chemistry C*, 2018, **6**, 6905-6910.
14. D. Kiefer, A. Giovannitti, H. Sun, T. Biskup, A. Hofmann, M. Koopmans, C. Cendra, S. Weber, L. J. Anton Koster, E. Olsson, J. Rivnay, S. Fabiano, I. McCulloch and C. Müller, *ACS Energy Letters*, 2018, **3**, 278-285.
15. I. E. Jacobs, Y. Lin, Y. Huang, X. Ren, D. Simatos, C. Chen, D. Tjhe, M. Statz, L. Lai, P. A. Finn, W. G. Neal, G. D'Avino, V. Lemaur, S. Fratini, D. Beljonne, J. Strzalka, C. B. Nielsen, S. Barlow, S. R. Marder, I. McCulloch and H. Sirringhaus, *Advanced Materials*, 2022, **34**, 2102988.

16. S. N. Patel, A. M. Glaudell, K. A. Peterson, E. M. Thomas, K. A. O'Hara, E. Lim and M. L. Chabinyc, *Science Advances*, 2017, **3**, e1700434.
17. V. Vijayakumar, P. Durand, H. Zeng, V. Untilova, L. Herrmann, P. Algayer, N. Leclerc and M. Brinkmann, *Journal of Materials Chemistry C*, 2020, **8**, 16470-16482.
18. D. T. Duong, C. Wang, E. Antono, M. F. Toney and A. Salleo, *Organic Electronics*, 2013, **14**, 1330-1336.
19. A. Hamidi-Sakr, L. Biniek, J.-L. Bantignies, D. Maurin, L. Herrmann, N. Leclerc, P. Lévêque, V. Vijayakumar, N. Zimmermann and M. Brinkmann, *Advanced Functional Materials*, 2017, **27**, 1700173.
20. J. Hynynen, D. Kiefer, L. Yu, R. Kroon, R. Munir, A. Amassian, M. Kemerink and C. Müller, *Macromolecules*, 2017, **50**, 8140-8148.
21. W. Liu, L. Müller, S. Ma, S. Barlow, S. R. Marder, W. Kowalsky, A. Köhn and R. Lovrincic, *The Journal of Physical Chemistry C*, 2018, **122**, 27983-27990.
22. D. T. Scholes, P. Y. Yee, J. R. Lindemuth, H. Kang, J. Onorato, R. Ghosh, C. K. Luscombe, F. C. Spano, S. H. Tolbert and B. J. Schwartz, *Advanced Functional Materials*, 2017, **27**, 1702654.
23. A. R. Chew, R. Ghosh, Z. Shang, F. C. Spano and A. Salleo, *The Journal of Physical Chemistry Letters*, 2017, **8**, 4974-4980.
24. Y. Zhong, V. Untilova, D. Muller, S. Guchait, C. Kiefer, L. Herrmann, N. Zimmermann, M. Brosset, T. Heiser and M. Brinkmann, *Advanced Functional Materials*, 2022, **32**, 2202075.
25. P. Y. Yee, D. T. Scholes, B. J. Schwartz and S. H. Tolbert, *The Journal of Physical Chemistry Letters*, 2019, **10**, 4929-4934.
26. E. Lim, A. M. Glaudell, R. Miller and M. L. Chabinyc, *Advanced Electronic Materials*, 2019, **5**, 1800915.
27. S. Zokaei, D. Kim, E. Järsvall, A. M. Fenton, A. R. Weisen, S. Hultmark, P. H. Nguyen, A. M. Matheson, A. Lund, R. Kroon, M. L. Chabinyc, E. D. Gomez, I. Zozoulenko and C. Müller, *Materials Horizons*, 2022, **9**, 433-443.
28. H. Sirringhaus, P. J. Brown, R. H. Friend, M. M. Nielsen, K. Bechgaard, B. M. W. Langeveld-Voss, A. J. H. Spiering, R. A. J. Janssen, E. W. Meijer, P. Herwig and D. M. de Leeuw, *Nature*, 1999, **401**, 685-688.
29. J. Rivnay, R. Noriega, R. J. Kline, A. Salleo and M. F. Toney, *Physical Review B*, 2011, **84**, 045203.
30. R. Noriega, J. Rivnay, K. Vandewal, F. P. V. Koch, N. Stingelin, P. Smith, M. F. Toney and A. Salleo, *Nature Materials*, 2013, **12**, 1038-1044.
31. M. Mone, Y. Kim, S. Darabi, S. Zokaei, L. Karlsson, M. Craighero, S. Fabiano, R. Kroon and C. Müller, *ACS Applied Materials & Interfaces*, 2023, **15**, 28300-28309.
32. R. Xie, A. R. Weisen, Y. Lee, M. A. Aplan, A. M. Fenton, A. E. Masucci, F. Kempe, M. Sommer, C. W. Pester, R. H. Colby and E. D. Gomez, *Nature Communications*, 2020, **11**, 893.
33. R. Kroon, A. I. Hofmann, L. Yu, A. Lund and C. Müller, *Chemistry of Materials*, 2019, **31**, 2770-2777.

34. J. Hynynen, E. Järsvall, R. Kroon, Y. Zhang, S. Barlow, S. R. Marder, M. Kemerink, A. Lund and C. Müller, *ACS Macro Letters*, 2019, **8**, 70-76.
35. S. Tokito, P. Smith and A. J. Heeger, *Polymer*, 1991, **32**, 464-470.
36. J. Moulton and P. Smith, *Polymer*, 1992, **33**, 2340-2347.
37. J. Moulton and P. Smith, *Synthetic Metals*, 1991, **40**, 13-22.
38. Y. Cao, P. Smith and A. J. Heeger, *Polymer*, 1991, **32**, 1210-1218.
39. T. Degousée, V. Untilova, V. Vijayakumar, X. Xu, Y. Sun, M. Palma, M. Brinkmann, L. Biniek and O. Fenwick, *Journal of Materials Chemistry A*, 2021, **9**, 16065-16075.
40. D. Kiefer, L. Yu, E. Fransson, A. Gómez, D. Primetzhofer, A. Amassian, M. Campoy-Quiles and C. Müller, *Advanced Science*, 2017, **4**, 1600203.
41. S. H. K. Paleti, Y. Kim, J. Kimpel, M. Craighero, S. Haraguchi, C. Müller, *Unpublished*.
42. R. Kroon, D. Kiefer, D. Stegerer, L. Yu, M. Sommer and C. Müller, *Advanced Materials*, 2017, **29**, 1700930.
43. D. Scheunemann, E. Järsvall, J. Liu, D. Beretta, S. Fabiano, M. Caironi, M. Kemerink and C. Müller, *Chemical Physics Reviews*, 2022, **3**.
44. M. Moser, L. R. Savagian, A. Savva, M. Matta, J. F. Ponder, Jr., T. C. Hidalgo, D. Ohayon, R. Hallani, M. Reisjalali, A. Troisi, A. Wadsworth, J. R. Reynolds, S. Inal and I. McCulloch, *Chemistry of Materials*, 2020, **32**, 6618-6628.
45. D. Kiefer, R. Kroon, A. I. Hofmann, H. Sun, X. Liu, A. Giovannitti, D. Stegerer, A. Cano, J. Hynynen, L. Yu, Y. Zhang, D. Nai, T. F. Harrelson, M. Sommer, A. J. Moulé, M. Kemerink, S. R. Marder, I. McCulloch, M. Fahlman, S. Fabiano and C. Müller, *Nature Materials*, 2019, **18**, 149-155.
46. R. J. Mammone and A. G. MacDiarmid, *Journal of the Chemical Society, Faraday Transactions 1: Physical Chemistry in Condensed Phases*, 1985, **81**, 105-112.
47. C. Müller, *Chemistry of Materials*, 2015, **27**, 2740-2754.
48. A. Lund, N. M. van der Velden, N.-K. Persson, M. M. Hamedi and C. Müller, *Materials Science and Engineering: R: Reports*, 2018, **126**, 1-29.